Separation Science and Technology
Publication details, including instructions for authors and subscription information:
http://www.informaworld.com/smpp/title~content=t713708471

Examination of the Adsorption of Large Biological Molecules to Anion Exchange Surfaces Using Surface Plasmon Resonance

William Riordan[a]; Kurt Brorson[b]; Scott Lute[b]; Mark Etzel[a]
[a] Department of Chemical and Biological Engineering, University of Wisconsin, Madison, WI, USA [b] Division of Monoclonal Antibodies, CDER/FDA, Silver Spring, MD, USA

Online publication date: 07 January 2010

To cite this Article Riordan, William , Brorson, Kurt , Lute, Scott and Etzel, Mark(2010) 'Examination of the Adsorption of Large Biological Molecules to Anion Exchange Surfaces Using Surface Plasmon Resonance', Separation Science and Technology, 45: 1, 1 — 10
To link to this Article: DOI: 10.1080/01496390903401770
URL: http://dx.doi.org/10.1080/01496390903401770

Separation Science and Technology, 45: 1–10, 2010

ISSN: 0149-6395 print/1520-5754 online
DOI: 10.1080/01496390903401770

Taylor & Francis
Taylor & Francis Group

Examination of the Adsorption of Large Biological Molecules to Anion Exchange Surfaces Using Surface Plasmon Resonance

William Riordan,[1] Kurt Brorson,[2] Scott Lute,[2] and Mark Etzel[1]
[1]*Department of Chemical and Biological Engineering, University of Wisconsin, Madison, WI, USA*
[2]*Division of Monoclonal Antibodies, CDER/FDA, Silver Spring, MD, USA*

Separation of viruses and other contaminants from protein therapeutics using anion exchange membrane adsorbers is a successful new approach to viral clearance; however, the fundamental phenomena that control performance are not well understood. For example, the kinetics of adsorption to the anion exchange surface may limit clearance, but has yet to be characterized experimentally and mathematically. In the present study, surface plasmon resonance was used to determine the adsorption kinetics for five large biological molecules: phage PP7, phage ΦX174, phage PR772, thyroglobulin, and DNA. Rate constants were incorporated into a kinetic model of chromatography to illustrate the impact on performance.

Keywords adsorption kinetics; anion exchange chromatography; bioseparations; mass transfer limitations; surface plasmon resonance; viral clearance

INTRODUCTION

Anion exchange membrane adsorbers are an important emerging technology for the purification of biological molecules (1,2). These devices consist of microporous membranes functionalized by attachment of a positively charged quaternary amine (Q) ligand that binds to negatively charged biological molecules in solution. Unlike traditional chromatography beads, which are frequently limited by slow intra-pore diffusion, mass transfer rates for membrane adsorbers are rapid because binding sites are located on membrane pores within the convective flow path of the feed solution. This makes the membrane adsorbers particularly attractive for large, slow-diffusing biological molecules, including large proteins (3,4), viruses (5,6), and DNA (7–9). Of particular interest is the application of anion exchange membrane adsorbers for viral clearance during the final polishing of recombinant protein therapeutics (10–15). These studies have shown that Q membrane adsorbers are effective for viral clearance independent of the flow rate, but that viral clearance can decrease significantly at increased feed solution salt concentrations (50–150 mM).

Despite the widespread use of anion exchange membrane adsorbers in biotechnology, a quantitative fundamental understanding of the system is still incomplete. The performance of anion exchange membrane adsorbers can be affected by a number of factors. For example, the shape of the breakthrough curve (BTC) may be determined by adsorption kinetics, the adsorption isotherm, the rate of mass transfer, flow mal-distribution, and flow dispersion. Without identifying the relative contributions of each of these factors, an accurate mathematical model of anion exchange membrane adsorbers cannot be developed. This represents an important problem, as an accurate mathematical model is critical for the understanding and prediction of chromatographic performance for important industrial separations such as viral clearance.

A prospective mathematical model for membrane adsorbers assumes slow adsorption kinetics limit the chromatographic performance. In this case, a kinetic model of chromatography based on the continuity equation and the Langmuir model of adsorption kinetics can be used to simulate BTCs for membrane adsorbers. Chromatographic performance is characterized by the dimensionless number of transfer units, n, given by (16,17):

$$n = \frac{(1-\varepsilon)k_a c_l L}{\varepsilon v} \tag{1}$$

The membrane porosity (ε), capacity (c_l), thickness (L), and interstitial flow velocity (v) are all measurable known quantities. The association rate constant (k_a), however, is generally unknown and must be estimated by fitting the model to BTC data. However, many factors determine the BTC shape, and fitting the BTC does not necessarily

Received 22 October 2008; accepted 7 August 2009.
Address correspondence to William Riordan, Department of Chemical and Biological Engineering, University of Wisconsin, 1605 Linden Drive, Madison, WI 53706, USA. E-mail: wtriordan@gmail.com

provide a true estimation of the intrinsic adsorption kinetics. Therefore, simply fitting the kinetic model of chromatography to BTC data does not answer the question as to whether adsorption kinetics are the performance-controlling step when using membrane adsorbers for different bioseparations.

A more straightforward method is to evaluate anion exchange adsorption kinetics and determine the adsorption association rate constant by means of surface plasmon resonance (SPR). Using this technique, the adsorption of the biological molecule to the ligand-functionalized surface is correlated to a change in refractive index at the surface, resulting in a real-time SPR response signal. The SPR signal is recorded on a sensorgram that can then be fit by a kinetic adsorption model to estimate the association rate constant. This rate constant can then be incorporated into the kinetic model equation (Eqn. 1) to simulate chromatographic performance for bioseparations such as viral clearance.

In order for the SPR signal to represent intrinsic kinetic data, the rate of adsorption in the SPR flow channel must be free from mass transfer limitations. When mass transfer limitations are present in the SPR flow channel, the rate of adsorption as measured by the SPR signal is slower than the intrinsic kinetic rate of adsorption. From an experimental standpoint, this results in flow rate-dependent SPR data, with the rate of adsorption decreasing at slower flow rates due to the inability of slower flow rates to supply a constant amount of analyte to the surface.

SPR-based biosensors have been used previously to study a wide range of interacting molecules including antibodies, antigens, enzymes, glycoproteins, nucleic acids, drugs, cells, and viruses (18–23). These applications typically involve low ligand density, low feed solution concentrations, and slow adsorption kinetics; conditions at which mass transfer limitations are minimized. Few studies have examined the adsorption of large biological molecules onto high-density surfaces useful for chromatographic bioseparations (24). SPR experiments used to study bioseparations are particularly susceptible to mass transfer limitations in the flow channel due to the high ligand density on the SPR sensor chip surface, large feed solution concentrations, and fast adsorption kinetics associated with anion exchange interactions. The work presented herein provides an example of how SPR can be used to study adsorption kinetics for bioseparations and relate the kinetics to the performance of an actual device like an anion exchange membrane adsorber.

In this work, SPR was used to measure the rate of adsorption of five large biological molecules onto a Q-functionalized anion exchange surface: thyroglobulin (THY), DNA, phage PP7, phage ΦX174, and phage PR772. Initial experiments were conducted at four different flow rates to determine the conditions at which SPR sensorgrams were not affected by the rate of mass transfer. Mass transfer limitations were also assessed theoretically to ensure that measured SPR sensorgrams reflected intrinsic adsorption kinetics. Association rate constants for anion exchange adsorption were obtained by fitting the Langmuir model to the data. With these rate constants, the relative kinetics for each of the biological molecules adsorbing to the Q-functionalized surface were compared. Additionally, the adsorption of phage PR772 onto a surface functionalized with an alternative anion exchange ligand (TAEA) previously determined to be more salt tolerant than the Q ligand was measured (25). Finally, the rate constants for the three bacteriophages were used to assess the expected role adsorption kinetics play for viral clearance operations using anion exchange membrane adsorbers.

MATERIALS AND METHODS

Phage Preparation

Bacteriophages PP7 and PR772 were prepared using the agar overlay plate method (26–28). A mixture of 9 mL overlay agar, 2 mL mid-log phase host bacteria (*Pseudomonas aeruginosa* for phage PP7, *E. coli K12* for phage PR772), and 10^5 plaque forming units (pfu) of the phage were added to each of the 25 nutrient agar (PP7) or tryptic soy agar (PR772) 150 mm plates. After solidification, the plates were incubated overnight at 37°C to allow bacterial growth and semi-confluent lysis of the bacterial lawn by the phage. A crude phage solution was recovered by harvesting the phage from each plate by washing with 10 mL of PBS (phosphate buffer saline, pH 7.4) for 4 h with gentle agitation and filtered with a 0.45 μm pore size filter followed by a 0.22 μm pore size filter.

Bacteriophage ΦX174 was prepared using the broth culture method (27). Tryptic soy broth (1 L) was seeded with 1% (v/v) of a confluent *E. coli C* culture grown overnight at 37°C. The seeded broth culture was grown at 37°C for 2.5 h, reaching a cell density of about 10^8 bacteria/mL. Calcium chloride was added to the broth culture to a concentration of 3 mM and the culture was grown for an additional 10 min. About 5×10^{11} plaque forming units (pfu) of ΦX174 were spiked into the broth culture and allowed to propagate for 3 h at 37°C. The culture was centrifuged at low speed (4,000 g) to pellet the bacteria and the supernatant was discarded. The bacteria pellets were then resuspended in 50 mL of borate buffer (50 mM sodium borate, 10 mM EDTA, pH 9.2) and lysed by adding 75 mg/L lysozyme and stirring for 4 h at 22°C, followed by three freeze-thaw cycles. Cell debris was spun down at moderate speed (9,000 g) for 15 min, and the crude phage solution was filtered with a 0.45 μm pore size filter followed by a 0.22 μm pore size filter.

Crude phage solutions were centrifuged at 90,000 g for 2.5 h at 10°C to pellet the phage. The phage pellets were

resuspended in PBS (PP7 and PR772) or borate buffer (ΦX174) and filtered through a 0.22 μm pore size filter followed by a 0.1 μm pore size filter. CsCl was added to bring the density of the phage solution to 1.4 g/mL (PP7), 1.36 g/mL (ΦX174), or 1.3 g/mL (PR772) and the solution was ultracentrifuged for 20 h at 300,000 g. Phage bands (red for PP7, milky white for PR772 and ΦX174) were removed from the centrifuge tube using a syringe and needle, and the purified phage stock solutions were then dialyzed against three changes of PBS (PP7 and PR772) or borate buffer (ΦX174). The titer of each of the purified stock solutions was determined using standard agar overlay plate counts.

Ligand Immobilization

C1 sensor chips and the standard amine coupling kit were purchased from Biacore (Biacore, Uppsala, Swedan). The C1 sensor chip has a flat carboxymethylated gold surface and lacks the dextran matrix associated with other commonly used sensor chips. The C1 chip was selected for this study because it was the recommended chip for large analyte particles that may encounter mass transfer limitations from slow diffusion into a dextran matrix.

The amine coupling kit was used to activate the sensor chip surface during the immobilization procedure. The kit contained N-ethyl-N′-(3-dimethylaminopropyl) carbodiimide hydrochloride (EDC), N-Hydroxysuccinimide (NHS), and ethanol amine (EA). Immobilization of the adsorptive ligands onto the C1 sensor chip surface was accomplished by activating the sensor chip surface with a mixture of NHS and EDC that form a reactive ester on the surface, which in turn reacts with primary amines on the ligands. The ligands used in these experiments were (2-aminoethyl)trimethylammonium chloride (Aldrich, Milwaukee, WI), commonly referred to as Q ligand in chromatography; and the salt tolerant ligand candidate tris-2-aminoethyl amine (TAEA) (Aldrich, Milwaukee, WI). The immobilization procedure consisted of 15 μL injections of the activation mixture and 20 μL injections of 1.0 M aqueous ligand solution cycled 100 times at a flow rate of 5 μL/min. This procedure was necessary to achieve a high surface capacity due to the relatively slow immobilization reaction. Upon completion of the cycle, remaining activated esters on the surface were blocked using three 50 μL injections of EA solution.

One of the sensor chip flow cells was used as a control to account for the effects of bulk refractive index shift and nonspecific binding. This flow channel was activated as before and capped with EA without coming in contact with ligand solution.

A 10 mM HEPES buffer at pH 7.4 was used as the mobile phase buffer throughout the immobilization procedure. All liquids were filtered through a 0.22 μm pore size filter and vacuum degassed prior to use.

TABLE 1
Properties of the large biomolecules examined in the present work

Biomolecule	Diameter (nm)	D (cm^2/s)	pI
THY	20	2.5×10^{-7}	4.5
DNA	11–120	2.1×10^{-7}	<3
PP7	24–33	1.6×10^{-7}	4.3–4.9
X174	26–33	1.5×10^{-7}	6.7–7.0
PR772	64–82	6.1×10^{-8}	3.8–4.2

SPR Adsorption Experiments

Physical properties of the five large biomolecules examined in this work are summarized in Table 1 (4,29). Stock solutions of THY and DNA were made by dissolving crystalline thyroglobulin (Sigma-Aldrich, St. Louis, MO) or diluting concentrated fragmented herring sperm DNA (Promega, Madison, WI) in bisTris buffer (50 mM bisTris, pH 6) to concentrations of 1 mg/mL (THY) or 0.1 mg/mL (DNA) as determined by absorbance at 280 nm (THY) or 260 nm (DNA). Phage stock solutions were prepared as described above to a titer of about 10^{12} pfu/mL. Feed solutions used in SPR adsorption experiments were made by diluting the stock solutions in mobile phase buffer. Borate buffer (pH 9.2) was used as the mobile phase buffer for phage ΦX174 (pI 6.7–7.0) rather than bisTris buffer so that the phage was negatively charged and would bind to the positively charged Q-functionalized surface. Tween 20 was added to the feed solutions (0.015%) in order to reduce the effects of nonspecific binding to the control surface. Feed solutions were filtered through a 0.22 μm pore size filter and vacuum degassed prior to use.

SPR adsorption experiments were performed on the BIAcore 2000 (Biacore, Uppsala, Sweden). Experiments were carried out by injecting 250 μL of feed solution into the BIAcore sensor chip flow channel and monitoring the SPR response signal on the collected sensorgram. Mass transfer limitations in the flow channel were examined by varying the flow rate and adsorption kinetics were characterized at two different feed solution concentrations for each biological molecule. For the flow rate experiments, feed solutions of THY (0.1 mg/mL), DNA (0.001 mg/mL), or phage PP7 (10^{11} pfu/mL) were examined at flow rates of 10, 30, 60, and 100 μL/min. Adsorption kinetic experiments were conducted at the following feed solution concentrations: 1.0 and 0.1 mg/mL THY; 0.001 and 0.0001 mg/mL DNA; 10^{11} and 10^{12} pfu/mL PP7; 6×10^{11} and 6×10^{12} pfu/mL ΦX174; and 2×10^{11} and 2×10^{12} pfu/mL PR772.

Sensor Chip Regeneration

After each adsorption experiment, material bound to the sensor chip surface was removed using a regeneration cycle. The complete regeneration cycle consisted of a 150 μL injection of 2 M NaCl, a 20 μL injection of pepsin solution, and a second 150 μL injection of 2 M NaCl to remove residual bound material and any bound pepsin. Pepsin solution was prepared by dissolving crystalline pepsin (Sigma, St. Louis, MO) in 50 mM phosphoric acid at pH 2.5 to a concentration of 2 mg/mL. The pepsin solution was used to hydrolyze material strongly bound to the sensor chip surface.

Kinetic Parameter Estimation

SPR sensorgram data was collected at a sampling rate of 1 Hz. The control surface response was subtracted from the anion exchange surface response in order to eliminate the effects of bulk refractive index shift caused by changing from the mobile phase buffer to the feed solution. Additionally, binding may occur to the gold sensor chip surface or EA nonspecifically. Therefore, subtracting the control surface eliminates the proportion of nonspecifically bound material from the original signal.

Athena Visual Workbench software (Athena Visual Software, Inc. Madison, WI) was used to fit the Langmuir model to the data and estimate kinetic parameters. The Langmuir model of adsorption is expressed mathematically by:

$$\frac{dc_s}{dt} = k_a c(c_l - c_s) - k_d c_s \qquad (2)$$

where c_s is the adsorbed surface concentration, c is the solution concentration at the surface, c_l is the total surface capacity, k_a is the association rate constant, and k_d is the dissociation rate constant.

Two assumptions were made when fitting the SPR data with Eqn. (2). First, the solution concentration near the surface was assumed to be equal to the bulk feed solution concentration; this is only true when there are no mass transfer limitations in the system and adsorption is completely controlled by the adsorption kinetics. Second, because the model fitting was not sensitive to the estimated value of k_d, adsorption was assumed to be completely irreversible and k_d was assumed to be negligibly small relative to the association constant and could thus be set to zero in Eqn. (2) for the purposes of this study. Setting the dissociation constant to zero was justified experimentally because no detectable level of desorption was observed when washing the anion exchange surface with the mobile phase buffer following the adsorption of the analyte. This assumption reduced the number of adjustable parameters from three to two, leaving k_a and c_l as estimated model parameters.

RESULTS

In this section, the SPR results for anion exchange adsorption kinetics will be presented. First, the SPR experiments conducted at different flow rates will be used to illustrate when mass transfer limitations in the SPR flow channel affect the sensorgram, and how to design experiments to avoid these limitations. Next, these SPR experimental design considerations will be utilized to perform experiments for each biological molecule at two different feed solution concentrations in order to obtain reliable estimates of kinetic constants. Finally, the performance of an alternative anion exchange ligand (TAEA) will be compared to the Q ligand in terms of the adsorption kinetics and binding capacity in the presence of salt.

Evaluation of Mass Transfer Limitations

If the SPR sensorgram is not limited by the rate of mass transfer, then the flow rate should have no effect. To examine this hypothesis, the adsorption of a large protein (THY), DNA, and phage PP7 onto an SPR sensor chip surface functionalized with the quaternary amine (Q) anion exchange ligand was measured at four different flow rates: 10, 30, 60, and 100 μL/min. The SPR sensorgrams were normalized to the fitted surface capacity ($C_s = c_s/c_l$) for direct comparison. The sensorgrams for THY and PP7 were not a function of flow rate as shown in Figs. 1a and 1b. Therefore, the kinetics for THY and PP7 adsorption to the Q-functionalized surface were slow relative to the rate of mass transfer, allowing for the collection of intrinsic kinetic adsorption data at flow rates as low as 10 μL/min.

In contrast, the SPR sensorgrams for DNA in Fig. 1c were flow rate dependent. These DNA sensorgrams are an example of how the SPR signal can be influenced by the rate of mass transfer when the adsorption kinetics are fast. The rate of adsorption and amount of adsorbed material increased as the flow rate increased, particularly early in the adsorption process when the reaction rate was fastest. For example, at 50 s, the amount of DNA adsorbed at flow rates of 10 and 30 μL/min was 33% and 73%, respectively, of the amount adsorbed at a flow rate of 60 μL/min. Increasing the flow rate to 100 μL/min did not further increase the adsorption rate. Therefore, a flow rate of 60 μL/min or higher must be used to collect an SPR sensorgram that reflects intrinsic adsorption kinetics for DNA.

Estimation of Adsorption Rate Constants

SPR sensorgrams were obtained for adsorption of THY, DNA, phage PP7, phage ΦX174, and phage PR772 onto the Q-functionalized anion exchange surface (Fig. 2). THY and the three bacteriophages experiments were conducted at 10–30 μL/min; DNA was conducted at 60 μL/min to avoid mass transfer limitations in the flow channel as described in the previous section. The

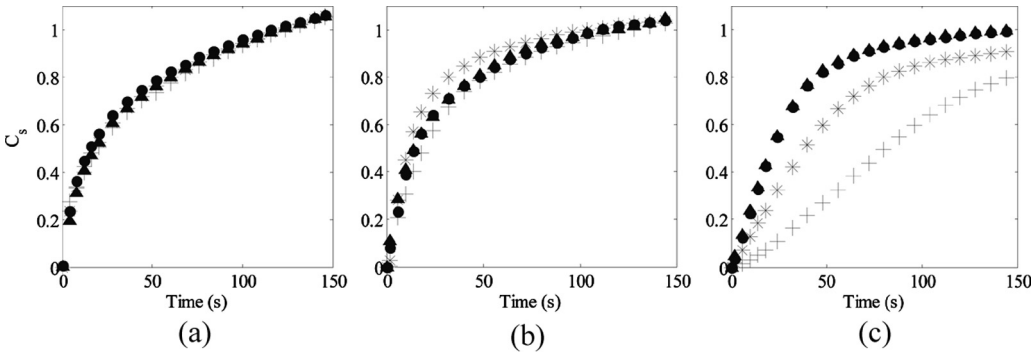

FIG. 1. SPR sensorgrams for (a) THY, (b) bacteriophage PP7, and (c) DNA onto the Q-functionalized surface. Experiments were conducted at flow rates of 10 (+), 30 (*), 60(•), and 100((▲) μL/min to evaluate the significance of mass transfer on the rate of adsorption.

sensorgrams were fit individually with the Langmuir model of adsorption (Eq. 1) in order to obtain the estimates of the association rate constant (k_a) and the SPR binding capacity (c_l).

The fitted parameter values for k_a and c_l for each experiment are given in Table 2. In most cases, the values for both of these parameters did not change by more than 1.25 fold with a 10-fold change in feed solution concentration. This was evidence that the Langmuir model effectively described the adsorption process. In one case (PR772), the variation in k_a with feed solution concentration was 1.6 fold, and in one other case (PP7) the variation in c_l was 1.6 fold. Nevertheless, the variation in either parameter value was always far less than the variation in the feed solution concentration. The fact that c_l generally did not decrease with the feed solution concentration provided evidence that experiments were being performed in the nonlinear region of the isotherm, supporting the assumption that anion exchange adsorption was essentially irreversible. The average values for k_a for both feed solution concentrations were as follows: THY = 0.2 mL/mg/s, DNA = 34 mL/mg/s, PP7 = 12 ×

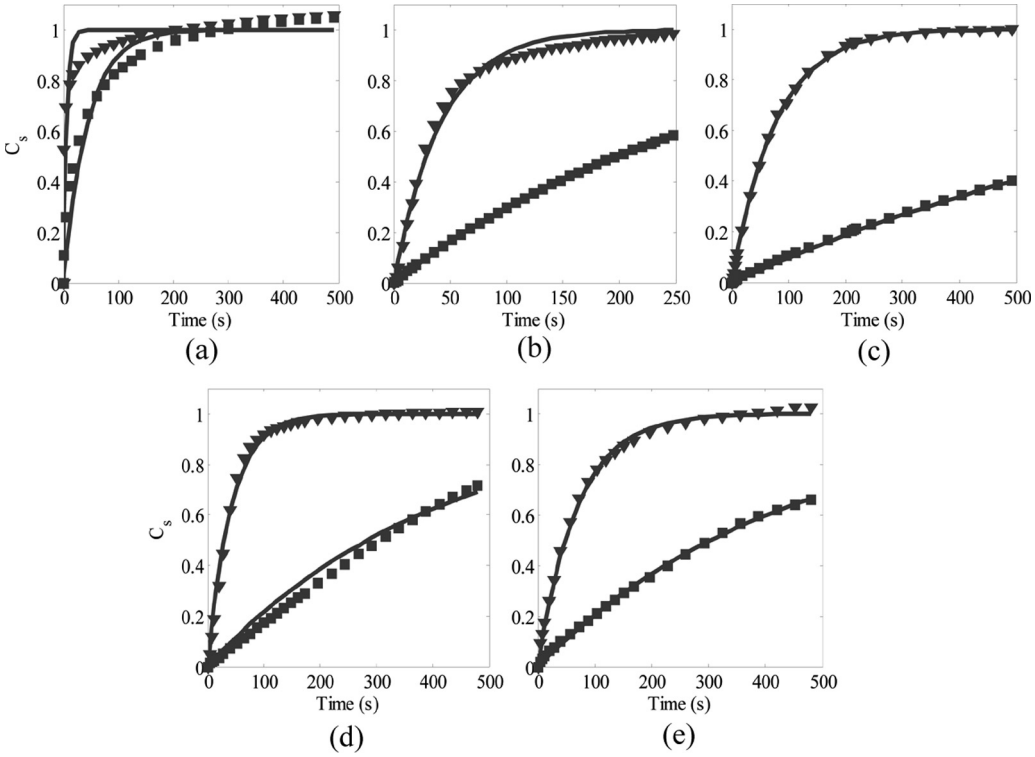

FIG. 2. SPR sensorgrams (symbols) and Langmuir model fits (solid lines) at two feed solution concentrations (see Table 2) for (a) THY, (b) DNA, (c) phage PP7, (d) phage ΦX174 and (e) phage PR772 onto the Q-functionalized surface.

TABLE 2
Kinetic parameter estimation results and calculated characteristic time for adsorption onto the Q-functionalized surface

	c_0 (mg/mL)	k_a (mL/mg/s)[1]	c_l (RU)[1]	t_{ads} (s)
THY	1.0	0.17 ± 0.02	1024 ± 5	5.9
	0.1	0.23 ± 0.01	1200 ± 6	43
DNA	0.001	33 ± 1	298 ± 2	30
	0.0001	35.2 ± 0.2	300 ± 1	280
	c_0 (pfu/mL)	k_a (mL/pfu/s)[1]	c_l (RU)[1]	t_{ads} (s)
PP7	1×10^{11}	$13 \pm 1 \times 10^{-14}$	1370 ± 1	77
	1×10^{10}	$10.3 \pm 0.4 \times 10^{-14}$	869 ± 3	970
ΦX174	6×10^{11}	$4.0 \pm 0.1 \times 10^{-14}$	563 ± 1	42
	6×10^{10}	$4.0 \pm 0.3 \times 10^{-14}$	513 ± 4	420
PR772	2×10^{11}	$8.1 \pm 0.1 \times 10^{-14}$	286 ± 1	62
	2×10^{10}	$13.3 \pm 0.1 \times 10^{-14}$	331 ± 3	380

[1]95% confidence interval based on nonlinear regression parameter estimation.

10^{-14} mL/pfu/s, ΦX174 $= 4 \times 10^{-14}$ mL/pfu/s, and PR772 $= 10 \times 10^{-14}$ mL/pfu/s. Because mass transfer limitations were shown to be minimal in this system, these rate constants reflect intrinsic adsorption kinetics between the biological molecule and the Q ligand.

The SPR sensorgrams and corresponding Langmuir model fits at two feed solution concentrations are shown in Fig. 2. Adsorption occurred much more slowly at the lower feed solution concentration for each of the biological molecules. The time scale of adsorption in each of the experiments can be compared by defining a characteristic adsorption time (t_{ads}):

$$t_{ads} = \frac{1}{k_a c_0}. \quad (3)$$

where k_a is the estimated association rate constant and c_0 is the feed solution concentration. The calculated t_{ads} for each sensorgram is provided in Table 2. Equation 3 can be used to calculate the required feed solution concentration to attain a desired adsorption time. For example, for $t_{ads} = 1$ s, s, the feed solution concentration for each of the biological molecules would have to be: THY = 5 mg/mL, DNA = 0.03 mg/mL, PP7 $= 9 \times 10^{12}$ pfu/mL, ΦX174 $= 3 \times 10^{13}$ pfu/mL, and PR772 $= 1 \times 10^{13}$ pfu/mL. Based on this analysis, DNA adsorption to the Q-functionalized surface is rapid; whereas THY would require a feed solution concentration 170 times larger than DNA to achieve the same characteristic adsorption time. The three viruses would also have to be in a highly concentrated feed solution ($\sim 10^{13}$ pfu/mL) to adsorb as quickly as DNA. A virus concentration of 10^{13} represents the practical upper limit of what can be prepared for bacteriophage; most virus feed solutions would be more dilute.

Considering a concentrated feed solution of 1 mg/mL (THY and DNA) or 10^{13} pfu/mL (bacteriophages), Eqn. 3 can be used to determine the relative of adsorption to the Q-functionalized surface: THY = 5.0 s, ΦX174 = 2.5 s, PR772 = 1.0 s, PP7 = 0.83 s, and DNA = 0.03 s. Based on this analysis, DNA has the fastest adsorption kinetics, followed by PP7, PR772, ΦX174, and finally THY.

Comparison of Adsorption to TAEA Ligand

Thus far, only the adsorption of different biological molecules onto a Q-functionalized surface has been considered. An alternative salt tolerant ligand, tris-2-aminoethyl) amine (TAEA), was compared to the Q ligand for adsorption of phage PR772. The estimated value of k_a for the TAEA-functionalized surface was 5.7×10^{-14} mL/pfu/s (data not shown), similar to the value of 8.1×10^{-14} mL/pfu/s determined for the Q-functionalized surface at the same feed solution concentration ($c_0 = 2 \times 10^{11}$ pfu/mL). The corresponding time scales for adsorption were also similar: Q = 62 s, and TAEA = 88 s. Therefore, anion exchange adsorption kinetics were the same for both anion exchange ligands, and both ligands would be expected to have the same chromatographic performance for separations described by Eqn. 1.

Finally, SPR was used to evaluate the binding capacity of surfaces functionalized with either Q or TAEA at different salt concentrations (0, 50, or 100 mM added salt). The normalized capacity, defined as amount bound with salt ÷ amount bound without salt, is shown in Fig. 3. The capacity of the Q-functionalized surface for PR772 was not statistically different when 50 mM salt was added to the feed solution ($p > 0.05$), maintaining 86% of its capacity. However, the capacity decreased significantly ($p < 0.05$) to only 21% of the initial value when 100 mM

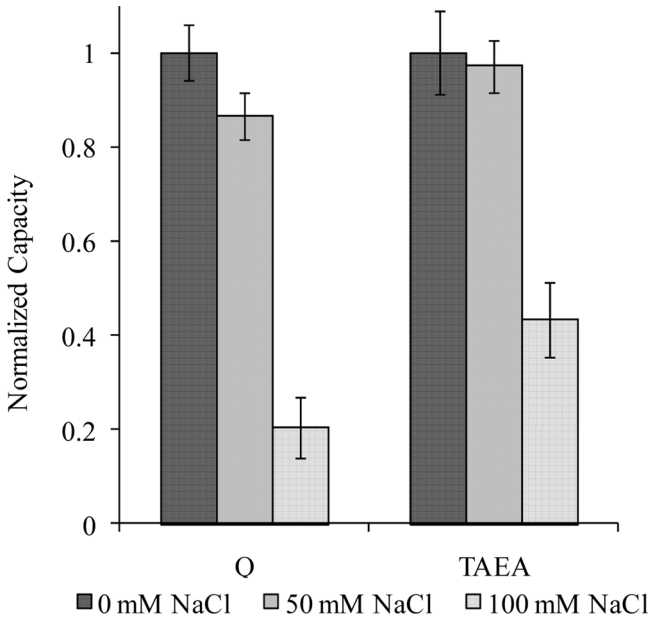

FIG. 3. Adsorption capacity of Q ligand and TAEA ligand surfaces for bacteriophage PR772 in feed solutions with 0, 50, and 100 mM added salt (error bars = SD, n = 2).

salt was added, respectively. The TAEA-functionalized surface maintained 97% and 43% of its capacity when 50 or 100 mM salt was added, respectively. The capacity of TAEA-functionalized surface for PR772 in 100 mM salt was substantially higher than the Q-functionalized surface ($p < 0.05$), demonstrating that the TAEA ligand was more salt tolerant. Based on this analysis, the alternative TAEA ligand was able to maintain a higher percentage of its binding capacity in higher salt conditions than the Q ligand, making it a better choice for bioseparations performed at elevated salt concentration.

DISCUSSION

In this section, the importance of mass transfer limitations on the SPR sensorgram will be illustrated by analysis of the experimental results using the convection-diffusion-reaction mathematical model of the SPR flow channel. In addition, the estimated kinetic rate constants determined from the SPR experiments will be incorporated into the kinetic model of chromatography to illustrate the likely importance of adsorption kinetics in bioseparations.

The impact of mass transfer limitations on the SPR sensorgram has been studied extensively using the convection-diffusion-reaction model (30–35). However, none of these reports addressed the unique situation encountered in bioseparation systems involving high ligand capacity, fast adsorption kinetics, and concentrated feed solutions. In a recent work by Riordan (2008), mass transfer limitations in the flow channel were characterized for bioseparations applications by the Peclet number (*Pe*) and the Dahmkohler number (*Da*), given mathematically by:

$$Pe = \frac{\text{convection}}{\text{diffusion}} = \frac{6Q}{wD} \tag{4}$$

$$Da = \frac{\text{reaction}}{\text{diffusion}} = \frac{k_a c_l h}{D} \tag{5}$$

where Q is the flow rate (Table 3), w is the channel width (=0.05 cm), D is the diffusion coefficient (Table 1), h is the channel height (=0.005 cm), k_a is the association rate constant (Table 2), and c_l is the surface capacity (Table 2) (36).

Solutions to the convection-diffusion-reaction model were compared to solutions of the Langmuir kinetic model to show the impact of mass transfer limitations. The sensorgram was considered under kinetic control when the amount bound calculated from the convection-diffusion-reaction model was 75% (upper critical *Da* in Table 3) to 95% (lower critical *Da* in Table 3) of the amount bound calculated from the Langmuir kinetic model at the midpoint. The midpoint was defined as the time where the amount bound was 50% of the amount bound at equilibrium ($t_{\text{midpoint}} = t_{\text{ads}} \times ln(2)$). The midpoint criterion was chosen as a compromise between two limiting extremes. At shorter times, the deviation was greater, because the adsorption rate was faster than the rate of

TABLE 3
Critical and experimental values for dimensionless Dahmkohler (*Da*) and Peclet (*Pe*) numbers

		Critical *Da**		Experimental *Da*	
Flow Rate (μL/min)	*Pe*	Lower	Upper	THY	DNA
10	8.0×10^4	0.21	1.2	0.37	7.6
30	2.4×10^5	0.47	3.0	0.36	15.5
60	4.8×10^5	0.68	4.0	0.34	20.5
100	8.0×10^5	0.94	6.1	0.30	22.1

*Theoretical critical *Da* based on the 95% (lower) and 75% (upper) criteria for the amount bound.

transport to the surface, causing the sensorgram to be limited by mass transfer. At longer times, the adsorption rate was slower than the transport rate, causing the sensorgram to be limited by kinetics.

Large values of *Da* reflect fast adsorption kinetics. In this case, mass transfer may limit the sensorgram because the transport rate may not be fast enough to replenish the analyte to the chip surface and maintain the liquid phase concentration at the feed solution value. Large values of *Pe* represent a high rate of convection and serve to thin the boundary layer and fully supply analyte to the chip surface. As *Da* increases, *Pe* must also increase to avoid obtaining a mass transfer limited sensorgram. Mass transfer and not intrinsic adsorption kinetics limit a flow rate dependent sensorgram.

The values of *Pe* Eq. (4) and *Da* Eq. (5) for THY and DNA adsorption to the Q-functionalized surface based on the parameter estimation results in Table 2 are provided in Table 3. For THY, the experimental *Da* did not change with increasing *Pe* (increasing flow rate), therefore the system was found experimentally not to be affected by the rate of the mass transfer. The experimental *Da* of 0.30–0.37 represents the intrinsic kinetics of the THY adsorption process. According to the convection-diffusion-reaction model, the mass transfer should not limit a system having an experimental *Da* that is smaller than the theoretical critical *Da*. This was what was observed experimentally. The experimental *Da* was smaller than the theoretical upper critical *Da* (75% criterion) at all flow rates, and smaller than the theoretical lower critical *Da* (95% criterion) at all flow rates except 10 μL/min (Table 3). Thus, the model simulations were in reasonably good agreement with the experimental observation that THY adsorption to the Q-functionalized surface was limited by adsorption kinetics.

For DNA, the experimental *Da* did not change with increasing Pe at flow rates of 60–100 μL/min, but did increase with increasing Pe at flow rates of 10–30 μL/min. Experimentally, the system transitioned from being mass transfer limited at the two low flow rates (10 and 30 μL/min) to being under kinetic control at the higher flow rates (60 and 100 μL/min). The experimental *Da* was greater than both the theoretical upper and lower critical *Da* at all flow rates, meaning that according to the model all of the DNA sensorgrams should have been limited by mass transfer. This was what was found for the two lowest flow rates, but not for the two highest flow rates. Based on this analysis, the predictions for mass transfer limitations in the SPR flow channel made using the model are slightly conservative. In other words, if there are no mass transfer limitations in the flow channel based on the model then there are not. However, there may also not be mass transfer limitations at even lower flow rates. Experimental evidence is needed to determine the impact of mass transfer in this case.

Once intrinsic kinetic adsorption data has been collected using SPR, the determined association rate constants can be used to predict the kinetic limit of performance of anion exchange membrane adsorbers a priori. Heister and Vermeulen (1952) found a simple algebraic solution for the BTC in the case of irreversible adsorption in the absence of axial dispersion, mass transfer limitations, and mixing in the flow system. This model was derived from the continuity equation using Langmuir adsorption kinetics as the constitutive relation (37):

$$C = \frac{1}{1 + (1 - e^{-n})e^{n(1-T)}} \tag{6}$$

where $C = c/c_0$, c is the effluent concentration, c_0 is the feed solution concentration, n is the dimensionless number of transfer units, and T is the dimensionless throughput parameter:

$$T = \frac{\varepsilon c_o}{(1-\varepsilon)c_l}(\tau - 1) \tag{7}$$

where the dimensionless time $\tau = vt/L$. T is a measure of membrane loading; the amount of solute loaded into the membrane via the feed solution versus the maximum amount of solute that can bind to the membrane.

Consider the application of membrane adsorbers to viral clearance, characterized by the log reduction value (LRV) of virus provided by the membrane adsorber. Based on the kinetic model of chromatography, the maximum LRV obtainable by a membrane adsorber is found from Eq. (8) (17):

$$LRV = -\log_{10} C \approx \frac{n(1-T)}{\ln(10)} \tag{8}$$

Thus, LRV is large for large n and small T. For viral clearance operations, the amount of virus loaded into the membrane is small compared to the membrane binding capacity ($T \approx 0$), and LRV is determined primarily by the parameter n.

As an example case, consider a membrane adsorber with properties in the range suggested by Suen and Etzel (1992): capacity (c_l) of 158 μM, thickness (L) of 250 μm, and membrane porosity (ε) of 0.7 (16). The operating flow velocity for membrane adsorbers during viral clearance should be rapid to maintain a high volumetric throughput rate; for this example, an interstitial flow velocity of 900 cm/h will be used to mirror the experimental conditions recommended by Phillips et al. (2005) for viral clearance (10). Based on these operating parameters, the predicted values of n (Eqn. 1) and LRV (Eqn. 8) for the three viruses are: PP7, $n = 489$, 212 LRV; ΦX174, $n = 163$, 71 LRV; and PR772, $n = 408$, 177 LRV.

The target for practical viral clearance validation studies is a demonstration of 4–6 LRV of the virus. In the work of

Phillips et al. (2005), clearance of different mammalian viruses and bacteriophage ranged from 5–7 LRV, and clearance was found to be independent of the flow rate. Based on the SPR analysis in the current work, anion exchange membrane adsorbers would be expected to provide complete clearance of the virus independent of interstitial flow velocity (up to 900 cm/hr), where the predicted LRV (LRV ≥ 70) far exceeds the limit of detection of experimental systems (LRV $\approx$ 12). This result is in partial agreement with the results obtained by Phillips et al. (2005). In both studies, viral clearance is independent of the flow rate, indicating adsorption kinetics are not rate-limiting for viral clearance; however, the incomplete clearance observed experimentally cannot be explained using SPR. These lower LRVs obtained experimentally should not be attributed to slow adsorption kinetics; rather, other factors such as virus micro-heterogeneity or non-ideal flow properties must be considered to explain insufficient viral clearance by anion exchange membrane adsorbers.

The kinetic rate constants determined from SPR can be used to determine when adsorption kinetics would be rate-limiting for anion exchange membrane adsorbers. Based on model simulations, kinetics are important for values of $n \leq 30$, corresponding to 13 LRV (17). Using the estimated associated rate constants from SPR, the required binding capacity (c_l) to avoid kinetic limitations can be calculated using Eqns. 1 and 8 ($n \leq 30$). For example, the required binding capacity for ΦX174 must be at least 29 μM to avoid kinetic limitations, whereas THY must have a binding capacity of at least 5200 μM. Therefore, separations involving THY are likely limited by adsorption kinetics, because the required capacity is 30-fold higher than the practical value of 158 μM. For ΦX174, adsorption kinetics are likely not rate limiting, as the calculated required capacity of 29 μM is less than the value of 158 μM. However, because 29 μM is on the same order of magnitude as 158 μM, any decrease in available binding capacity could cause the system to become kinetically limited.

These calculations reveal an important point for viral clearance: even though the membrane adsorber is removing only trace levels of the virus, the binding capacity is still an important design consideration. Based on Eqs. (1) and (8), only membranes with large binding capacities will result in large values of the LRV. These equations are not a function of feed solution concentration when $T \approx 0$, as in most viral clearance studies. Therefore, it is critical that the membranes have a high capacity regardless of the virus concentration in the feed solution. High capacity is particularly important due to the complex mixture of impurities with which membranes are challenged; competitive binding between viruses, DNA, and host cell protein that are also present in the feed solution could lower the apparent binding capacity, decrease n, and slow the apparent adsorption kinetics for the virus. Lowered capacity would also increase T, lowering clearance if T approaches one. Therefore, because of the stringent requirements on viral clearance, increases in binding capacity are sought after during the development of membrane adsorbers for viral clearance applications.

CONCLUSIONS

In this study, SPR was shown to be an effective tool for the examination of adsorption of large biological molecules onto surfaces functionalized with anion exchange ligands. Using SPR, intrinsic kinetic data can be obtained free of mass transfer limitations that can be used to estimate the association rate constant for adsorption to the anion exchange surface. Based on subsequent analysis of the estimated rate constants for DNA and three viruses, anion exchange adsorption kinetics are ordinarily fast enough to not limit DNA and viral clearance: predicted clearance is much larger than what is measured experimentally. The SPR data and model calculations were used to illustrate when the adsorption kinetics would and would not limit viral clearance, and illustrated the importance of membrane binding capacity to avoid these kinetic limitations. In conclusion, SPR was shown to be an effective tool for the study of adsorptive bioseparations, and was utilized to demonstrate the role of adsorption kinetics in viral clearance operations using anion exchange membrane adsorbers.

REFERENCES

1. Avramescu, M.; Borneman, Z.; Wessling, M. (2003) Dynamic behavior of adsorber membranes for protein recovery. *Biotechnol. Bioeng.*, *84*: 564–572.
2. Ghosh, R. (2002) Protein separation using membrane chromatography: opportunities and challenges. *J. Chromatogr. A*, *952*: 13–27.
3. Suck, K.; Walter, J.; Menzel, F.; Tappe, A.; Kasper, C.; Naumann, C.; Zeidler, R.; Scheper, T. (2006) Fast and efficient protein purification using membrane adsorber systems. *J. Biotechnol.*, *121*: 361–367.
4. Yang, H.; Viera, C.; Fischer, J.; Etzel, M.R. (2002) Purification of a large protein using ion-exchange membranes. *Ind. Eng. Chem. Res.*, *41*: 1597–1602.
5. Han, B.; Specht, R.; Wickramasinghe, S.; Carlson, J. (2005) Binding Aedes aegypti densonucleosis virus to ion exchange membranes. *J. Chromatog. A*, *1092*: 114–124.
6. Kalbfuss, B.; Wolff, M.; Geisler, L.; Tappe, A.; Wickramasinghe, R.; Thom, V.; Reichl, U. (2007) Direct capture of influenza A virus from cell culture supernatant with Sartobind anion-exchange membrane adsorbers. *J. Membrane Sci.*, *299*: 251–260.
7. Endres, H.N.; Johnson, Julie, A.C.; Ross, C.A.; Welp, J.K.; Etzel, M.R. (2003) Evaluation of an ion-exchange membrane for the purification of plasmid DNA. *Biotechnol. Appl. Biochem.*, *37*: 259–266.
8. Montesinos-Cisneros, R.; Olivas, J.; Ortega, J.; Guzman, R.; Tejeda-Mansir, A. (2007) Breakthrough performance of plasmid DNA on ion-exchange membrane columns. *Biotechnol. Prog.*, *23*: 881–887.
9. Teeters, M.A.; Conrardy, S.E.; Thomas, B.L.; Root, T.W.; Lightfoot, E.N. (2003) Adsorptive membrane chromatography for purification of plasmid DNA. *J. Chromatogr. A*, *989*: 165–173.
10. Phillips, M.; Cormier, J.; Ferrence, J.; Dowd, C.; Kiss, R.; Lutz, H.; Carter, J. (2005) Performance of a membrane adsorber for trace

impurity removal in biotechnology manufacturing. *J. Chromatogr. A*, *1078*: 74–82.
11. Knudsen, H.L.; Fahrner, R.L.; Xu, Y.; Norling, L.A.; Blank, G.S. (2001) Membrane ion-exchange chromatography for process-scale antibody purification. *J. Chromatogr. A*, *907*: 145–154.
12. Gottschalk, U. (2005) Downstream processing of monoclonal antibodies: from high dilution to high purity. *Biopharm. Intern.*, *18*: 42–52.
13. Boi, C. (2007) Membrane adsorbers as purification tools for monoclonal antibody purification. *J. Chromatogr. B*, *848*: 19–27.
14. Zhou, J.; Solamo, F.; Hong, T.; Shearer, M.; Tressel, T. (2008) Viral clearance using disposable systems in monoclonal antibody commercial downstream processing. *Biotech. Bioeng.*, *100*: 488–496.
15. Zhou, J.X.; Tressel, T. (2006) Basic concepts in Q membrane chromatography for large-scale antibody production. *Biotechnol. Prog.*, *22*: 341–349.
16. Suen, S.; Etzel, M.R. (1992) A mathematical analysis of affinity membrane bioseparations. *Chem. Eng. Sci.*, *47*: 1355–1364.
17. Etzel, M.; Riordan, W. (2007) Membrane chromatography: analysis of breakthrough curves and viral clearance. In: *Process Scale Bioseparations for the Biopharmaceutical Industry*, Shukla, A.; Etzel, M.; Gadam, S. eds.; CRC Press: Boca Raton, Fl, 277–296.
18. Karlsson, R. (2004) SPR for molecular interaction analysis: a review of emerging application areas. *J. Mol. Recognit.*, *17*: 151–161.
19. Nygren-Babol, L.; Sternesjo, A.; Jagerstad, M.; Bjorck, L. (2005) Affinity and rate constants for interactions of bovine folate-binding protein and folate derivatives determined by optical biosensor technology. Effect of stereoselectivity. *J. Agric. Food Chem.*, *53*: 5473–5478.
20. Quinn, J.G.; O'Kennedy, R. (2001) Biosensor-based estimation of kinetic and equilibrium constants. *Anal. Biochem.*, *290*: 36–46.
21. Rich, R.; Day, Y.; Morton, T.; Myszka, D. (2001) High-resolution and high-throughput protocols for measuring drug/human serum albumin interactions using BIACORE. *Anal. Biochem.*, *296*: 197–207.
22. Ashish, B.; Murthy, G. (2004) Analysis of human chorionic gonadotropin-monoclonal antibody interaction in BIAcore. *J. Biosci.*, *29*: 57–66.
23. Qureshi, M.H.; Wong, S. (2002) Design, production, and characterization of a monomeric streptavidin and its application for affinity purification of biotinylated proteins. *Prot. Expression Purif.*, *25*: 409–415.
24. Hall, D. (2001) Use of optical biosensors for the study of mechanistically concerted surface adsorption processes. *Anal. Biochem.*, *288*: 109–125.
25. Johansson, B.; Belew, M.; Eriksson, S.; Glad, G.; Lind, O.; Maloisel, J.; Norrman, N. (2003) Preparation and characterization of prototypes for multi-modal separation media aimed at the capture of negatively charged biomolecules at high salt conditions. *J. Chromatogr. A*, *1016*: 21–33.
26. Brorson, K.; Sofer, G.; Robertson, G.; Lute, S.; Martin, J.; Aranha, H.; Haque, M.; Satoh, S.; Yoshinari, K.; Moroe, I.; Morgan, M.; Yamaguchi, F.; Carter, J.; Krishnan, M.; Stefanyk, J.; Etzel, M.; Riordan, W.; Korneyeva, M.; Sundaram, S.; Wilkommen, H.; Wojciechowski, P. (2005) "Large pore size" virus filter test method recommended by the PDA virus filter task force. *PDA J. Pharm. Sci. Technol.*, *59*: 177–186.
27. Lute, S.; Bailey, M.; Combs, J.; Sukumar, M.; Brorson, K. (2007) Phage passage after extended processing in small-virus-retentive filters. *Biotechnol. Appl. Biochem.*, *47*: 141–151.
28. Lute, S.; Aranha, H.; Tremblay, D.; Liang, D.; Ackermann, H.; Chu, B.; Moineau, S.; Brorson, K. (2004) Characterization of coliphage PR772 and evaluation of its use for virus filter performance testing. *Appl. Environ. Microbiol.*, *70*: 4864–4871.
29. Brorson, K.; Shen, H.; Lute, S.; Perez, J.S.; Frey, D. (2008) Characterization and purification of bacteriophages using chromatofocusing. *J. Chromatogr. A*, *1207*: 110–121.
30. Yarmush, M.L.; Patankar, D.B.; Yarmush, D.M. (1996) An Analysis of transport resistances in the operation of BIAcore; implications for kinetic studies of biospecific interactions. *Mol. Immun.*, *33*: 1203–1214.
31. Schuck, P.; Minton, A.P. (1996) Analysis of mass transport-limited binding kinetics in evanescent wave biosensors. *Anal. Biochem.*, *240*: 262–272.
32. Sikavitsas, V.; Nitsche, J.M.; Mountziaris, T.J. (2002) Transport and kinetic processes underlying biomolecular interactions in the BIAcore optical biosensor. *Biotechnol. Prog.*, *18*: 885–897.
33. Myszka, D.G.; He, X.; Dembo, M.; Morton, T.A.; Goldstein, B. (1998) Extending the range of rate constants available from BIAcore: interpreting mass transport-influenced binding data. *Biophys. J.*, *75*: 583–594.
34. Goldstein, B.; Coombs, D.; He, X.; Pineda, A.R.; Wofsy, C. (1999) The influence of transport on the kinetics of binding to surface receptors: application to cells and BIAcore. *J. Mol. Recognit.*, *12*: 293–299.
35. Glaser, R.W. (1993) Antigen-antibody binding and mass-transport by convection and diffusion to a surface–a 2-dimensional computer model of binding and dissociation kinetics. *Anal. Biochem.*, *213*: 152–161.
36. Riordan, W. (2008) Analysis and Design of Membrane Adsorbers for Viral Clearance. Ph.D. Diss., University of Wisconsin–Madison.
37. Heister, N.K.; Vermeulen, T. (1952) Saturation performance of ion-exchange and adsorption columns. *Chem. Eng. Prog*, *48*: 505–516.